Astronomy & Astrophysics manuscript no. AA-2013-22951
November 1, 2013

Contemporaneous observations of the radio galaxy NGC 1275 from radio to very high energy γ-rays

J. Aleksić[1], S. Ansoldi[2], L. A. Antonelli[3], P. Antoranz[4], A. Babic[5], P. Bangale[6], U. Barres de Almeida[6], J. A. Barrio[7], J. Becerra González[8], W. Bednarek[9], K. Berger[8], E. Bernardini[10], A. Biland[11], O. Blanch[1], R. K. Bock[6], S. Bonnefoy[7], G. Bonnoli[3], F. Borracci[6], T. Bretz[12,25], E. Carmona[13], A. Carosi[3], D. Carreto Fidalgo[12], P. Colin[6], E. Colombo[8], J. L. Contreras[7], J. Cortina[1], S. Covino[3], P. Da Vela[4], F. Dazzi[2], A. De Angelis[2], G. De Caneva[10], B. De Lotto[2], C. Delgado Mendez[13], M. Doert[14], A. Domínguez[15,26], D. Dominis Prester[5], D. Dorner[12], M. Doro[16], S. Einecke[14], D. Eisenacher[12], D. Elsaesser[12], E. Farina[17], D. Ferenc[5], M. V. Fonseca[7], L. Font[18], K. Frantzen[14], C. Fruck[6], R. J. García López[8], M. Garczarczyk[10], D. Garrido Terrats[18], M. Gaug[18], G. Giavitto[1], N. Godinović[5], A. González Muñoz[1], S. R. Gozzini[10], A. Hadamek[14], D. Hadasch[19], A. Herrero[8], D. Hildebrand[11], J. Hose[6], D. Hrupec[5], W. Idec[9], V. Kadenius[20], H. Kellermann[6], M. L. Knoetig[11], J. Krause[6], J. Kushida[21], A. La Barbera[3], D. Lelas[5], N. Lewandowska[12], E. Lindfors[20,27], S. Lombardi[3], M. López[7], R. López-Coto[1], A. López-Oramas[1], E. Lorenz[6], I. Lozano[7], M. Makariev[22], K. Mallot[10], G. Maneva[22], N. Mankuzhiyil[2], K. Mannheim[12], L. Maraschi[3], B. Marcote[23], M. Mariotti[16], M. Martínez[1], D. Mazin[6], U. Menzel[6], M. Meucci[4], J. M. Miranda[4], R. Mirzoyan[6], A. Moralejo[1], P. Munar-Adrover[23], D. Nakajima[21], A. Niedzwiecki[9], K. Nilsson[20,27], N. Nowak[6], R. Orito[21], A. Overkemping[14], S. Paiano[16], M. Palatiello[2], D. Paneque[6], R. Paoletti[4], J. M. Paredes[23], X. Paredes-Fortuny[23], S. Partini[4], M. Persic[23], F. Prada[15,28], P. G. Prada Moroni[24], E. Prandini[16], S. Preziuso[4], I. Puljak[5], R. Reinthal[20], W. Rhode[14], M. Ribó[23], J. Rico[1], J. Rodriguez Garcia[6], S. Rügamer[12], A. Saggion[16], T. Saito[21], K. Saito[21], M. Salvati[3], K. Satalecka[7], V. Scalzotto[16], V. Scapin[7], C. Schultz[16], T. Schweizer[6], S. N. Shore[24], A. Sillanpää[20], J. Sitarek[1], I. Snidaric[5], D. Sobczynska[9], F. Spanier[12], V. Stamatescu[1], A. Stamerra[3], T. Steinbring[12], J. Storz[12], S. Sun[6], T. Surić[5], L. Takalo[20], F. Tavecchio[3], T. Terzić[5], D. Tescaro[8], M. Teshima[6], J. Thaele[14], O. Tibolla[12], D. F. Torres[19], T. Toyama[6], A. Treves[17], M. Uellenbeck[14], P. Vogler[11], R. M. Wagner[6,29], F. Zandanel[15,30], R. Zanin[23] (*The MAGIC Collaboration*), and B. Balmaverde[31], J. Kataoka[32], R. Rekola[20], and Y. Takahashi[32]

(Affiliations can be found after the references)

Preprint online version: November 1, 2013

ABSTRACT

Aims. The radio galaxy NGC 1275, recently identified as a very high energy (VHE, >100 GeV) γ-ray emitter by MAGIC, is one of the few non-blazar active galactic nuclei detected in the VHE regime. The purpose of this work is to better understand the origin of the γ-ray emission and locate it within the galaxy.

Methods. We study contemporaneous multi-frequency observations of NGC 1275 and model the overall spectral energy distribution. We analyze unpublished MAGIC observations carried out between October 2009 and February 2010, and the already published observations taken between August 2010 and February 2011. We study the multi-band variability and correlations analyzing data of *Fermi*-LAT in the 100 MeV–100 GeV energy band, *Chandra* (X-ray), KVA (optical) and MOJAVE (radio) taken during the same period.

Results. Using custom Monte Carlo simulations corresponding to early MAGIC stereoscopic data, we detect NGC 1275 also in the earlier MAGIC campaign. The flux level and energy spectra are similar to the results of the second campaign. The monthly light curve above 100 GeV shows a hint of variability at the $3.6\,\sigma$ level. In the *Fermi*-LAT band, both flux and spectral shape variabilities are reported. The optical light curve is also variable and shows a clear correlation with the γ-ray flux above 100 MeV. In radio, three compact components are resolved in the innermost part of the jet. One of these components shows a similar trend as the *Fermi*-LAT and KVA light curves. The γ-ray spectra measured simultaneously with MAGIC and *Fermi*-LAT from 100 MeV to 650 GeV can be well fit either by a log-parabola or by a power-law with a sub-exponential cutoff for the two observation campaigns. A single-zone synchrotron-self-Compton model, with an electron spectrum following a power-law with an exponential cutoff, can explain the broadband spectral energy distribution and the multi-frequency behavior of the source. However, this model suggests an untypical low bulk Lorentz factor or a velocity alignment closer to the line of sight than the parsec-scale radio jet.

Key words. galaxies: active - galaxies: jets - galaxies: individual (NGC 1275/3C 84) - gamma rays: galaxies

1. Introduction

The radio galaxy NGC 1275 is the central dominant galaxy of the Perseus cluster (Abell 426). It is a well known active galactic nucleus (AGN) already included in the original study of Seyfert (1943). In fact, it is a rather complex object with very peculiar characteristics that could be the result of massive gas accretion from the cluster cooling flow or from a recent merging event (Conselice et al. 2001). The main features, in addition to the central AGN, are remarkable gas filaments that are tens of kpc long emitting strong hydrogen lines (Lynds 1970) and a foreground galaxy falling toward NGC 1275 (Caulet et al. 1992).

In radio, the emission is dominated by a very bright compact source (3C 84) at the center of the galaxy. The core-dominated morphology with asymmetrical jets at both kpc (Pedlar et al. 1990) and pc scales (Asada et al. 2006) looks like a Fanaroff-Riley type I (FR I) radio galaxy with a jet axis relatively close to the line of sight. The faint counter jet measured with Very Long Baseline Interferometry (VLBI) suggests a jet angle of 30°–55° in the core region (Vermeulen et al. 1994; Walker et al. 1994; Asada et al. 2006). At larger scales, there is evidence of jet bending (Pedlar et al. 1990). The flux and morphology of the core radio emission are variable. Recent observations showed that an outburst is on-going since 2005 (Nagai et al. 2010). At sub-pc scales, a new component appeared near the nucleus in 2007 and keeps growing in flux as it travels away from the nucleus. Since 2010, its brightness at 15 GHz has overtaken the nucleus (Nagai et al. 2012a).

The X-ray emission is dominated by the thermal emission of the intra-cluster medium cooling flow in the cluster central region (Churazov et al. 2003; Fabian et al. 2011). However, a non-thermal component from the nucleus is detected with high-resolution instruments (Churazov et al. 2003; Balmaverde et al. 2006) that follows a hard power-law spectrum (photon index Γ=1.6±0.1) in the 0.5–10 keV range. Non-thermal emission also appears in hard X-ray above ∼20 keV (Ajello et al. 2009; Eckert & Paltini 2009), that well matches the extrapolation of the AGN power-law X-ray emission.

In γ-rays, emission from both the cluster and the AGN was expected. A first hint of high-energy emission from the NGC 1275 region was found in the COS B data [1975–1982] (Strong & Bignami 1983) but was not confirmed by the next instrument *CGRO*-EGRET starting observation one decade later [1991–2000] (Reimer at al. 2003). After the first four months of all-sky survey with *Fermi*-LAT in 2008, γ-ray emission from NGC 1275 was clearly established (Abdo et al. 2009). The measured flux above 100 MeV was seven times higher than the *CGRO*-EGRET upper limit, suggesting strong variability of the source. Subsequent *Fermi*-LAT observations confirmed this variability, revealing variation time scales as rapid as a week (Kataoka et al. 2010; Brown & Adams 2011).

At very high energies (VHE, >100 GeV), NGC 1275 has been observed without success by many Cherenkov Telescope experiments: HEGRA (Goetting et al. 2001), Whipple-10 m (Perkins et al. 2006), VERITAS (Acciari et al. 2009) and MAGIC-I (Aleksić et al. 2010b). The first detection was recently reported by MAGIC in stereoscopic mode (Aleksić et al. 2012a). The 70–500 GeV energy spectrum is much steeper than the 0.1–20 GeV spectrum measured by *Fermi*-LAT, suggesting a break or a cutoff at a few tens of GeV. The angular resolution of the γ-ray telescopes is not sufficient to determine the origin of the emission within the galaxy, but the rapid variability seen by *Fermi*-LAT implies a very compact emission region, most likely from the inner part of the AGN. Additionally, the expected cluster γ-ray emission should extend over a region of several hundred kpc (Pinzke & Pfrommer 2010), and then must be constant on human timescales. This emission could be detectable when the AGN is quiet (Colafrancesco et al. 2010) or above the high energy cutoff of the AGN (Aleksić et al. 2012b).

In this work, we study contemporaneous multi-frequency observations of the AGN emission. We analyzed the MAGIC data taken in stereoscopic mode from October 2009 to February 2011 as well as *Fermi*-LAT data, X-ray *Chandra* data, optical data of KVA and NOT, and radio data of the MOJAVE programme at VLBA from the same observation period. Together with additional information from archival data, we discuss a possible emission scenario and try to model the source as a misaligned BL Lac object.

2. Observations and Data Analysis

2.1. MAGIC

MAGIC is a system of two 17 m-diameter imaging atmospheric Cherenkov telescopes located at the Roque de los Muchachos observatory (28.8°N, 17.8°W, 2200 m a.s.l.), on the Canary Island of La Palma. The MAGIC telescopes have been operating in stereoscopic mode since the autumn of 2009 with a sensitivity ≤0.8% of the Crab Nebula flux, for energies above ∼300 GeV, in 50 h of observations (Aleksić et al. 2012c). The trigger system, optimized for the lowest energies, gives the possibility to study γ-ray emission down to 50 GeV.

The MAGIC telescopes observed NGC 1275 during two distinct observational campaigns performed between October 2009 and February 2010 (∼45.3 h), and August 2010 and February 2011 (∼53.6 h), respectively. Both campaigns were carried out in stereoscopic mode, but under different global trigger configurations.

The first campaign (Camp. 1) happened partially during the commissioning phase of the second telescope (MAGIC-II). It was performed in the so-called soft-stereo trigger mode, with the first telescope (MAGIC-I) trigger working in single mode and the second telescope (MAGIC-II) recording only events triggered by both telescopes. This campaign resulted in the discovery of γ-ray emission above 300 GeV from IC 310, another radio galaxy of the Perseus cluster (Aleksić et al. 2010a, 2013).

In the second campaign (Camp. 2), observations were instead taken in the standard full-stereo trigger mode (recorded events are triggered simultaneously by both telescopes). It resulted in the first detection of NGC 1275 at energies above 100 GeV (Aleksić et al. 2012a).

The soft-stereo trigger allows us to analyze MAGIC-I data in single mode but has a slightly higher energy threshold for stereoscopic data than the full-stereo trig-

---

Send offprint requests to: Pierre Colin (colin@mppmu.mpg.de), Saverio Lombardi (saverio.lombardi@oa-roma.inaf.it), Fabrizio Tavecchio (fabrizio.tavecchio@brera.inaf.it), Dorothée Hildebrand (dorothee.hildebrand@phys.ethz.ch), Elina Lindfors (elilin@utu.fi)

ger. However, above ∼150 GeV data collected in both campaigns are almost identical and can be treated as a uniform data sample. This was done for the study of the γ-ray emission induced by cosmic-ray population in the Perseus cluster (Aleksić et al. 2012b). Instead, for data analysis below 150 GeV (as performed here), the two campaigns must be analyzed separately.

Both surveys were performed in the false source tracking (wobble) mode (Fomin et al. 1994), with data equally split in two (Camp. 1) or four (Camp. 2) pointing positions located symmetrically at 0.4° from NGC 1275. Observations were carried out at low zenith angles (<35°), which resulted in an analysis energy threshold (defined as the peak of the γ-ray energy distribution for a Crab-like spectrum) of 100 GeV.

The data analysis was performed using the standard software package MARS (Albert et al. 2008a; Aliu et al. 2009), including the latest standard routines for stereoscopic analysis (Aleksić et al. 2012c; Lombardi et al. 2011). The γ-ray selection cuts were optimized by means of contemporaneous Crab Nebula data and Monte Carlo simulations. The background is estimated from mirror regions (off-regions) corresponding to the source position in the camera during the other wobble pointing. Thus, depending on the number of wobble positions used in the campaign, a single off-region (Camp. 1) or three off-regions (Camp. 2) are considered. While the standard Monte Carlo simulations were used for the analysis of Camp. 2 data (already reported in Aleksić et al. 2012a), the data analysis of the first campaign required new dedicated simulations in order to fully take into account the non-standard trigger condition at the lowest energies (<150 GeV).

After the application of standard quality checks based on the rate of the stereo events and the distributions of basic image parameters, 39.0 h (Camp. 1) and 45.7 h (Camp. 2) of data were selected to derive the results presented here. The rejected data were affected mainly by non-optimal atmospheric conditions during the data taking.

The γ-ray signal from the NGC 1275 is detected only at low energies. Fig. 1 shows the θ^2 plot[1] obtained with Camp. 1 data (October 2009 – February 2010) for analysis cuts corresponding to an energy threshold of 100 GeV. We found an excess of 742±122 events in the fiducial signal region with $\theta^2 < 0.026\,\mathrm{degree}^2$, corresponding to a significance of 6.1 σ, calculated according to the Eq. 17 of Li & Ma (1983). During the second campaign (August 2010 – February 2011), an excess of 522±81 events above the same energy threshold was detected with a significance of 6.6 σ. Detailed Camp. 2 results are reported in Aleksić et al. (2012a).

The significance skymap above 100 GeV for the first campaign is shown in Fig. 2. The central hot spot (>6 σ) corresponding to the NGC 1275 position is consistent with a point-like source. Conversely to the skymap above 400 GeV reported in Aleksić et al. (2010a) for the same period, the radio galaxy IC 310 is not visible in the ∼100 GeV skymap due to its very hard spectrum.

The unfolded differential energy spectra of the source derived from the two observational campaigns are shown in Fig. 3. The error bars represent the statistical uncertainties only, but for the power-law fit parameterization the systematic effects[2] are also taken into account. For Camp. 1, the spectrum between 65 GeV and 650 GeV can be described by a simple power-law ($\chi^2/n_{dof} = 4.86/3$)

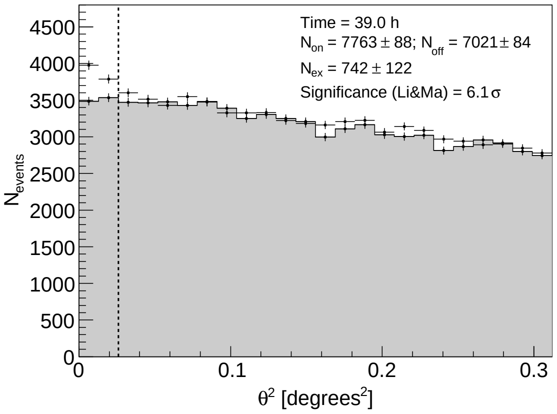

Fig. 1. θ^2 distributions of the NGC 1275 signal and background estimation from 39.0 h of MAGIC stereo observations taken between October 2009 and February 2010, in soft-trigger stereo mode (see 2.1) with an energy threshold of 100 GeV. The region between zero and the vertical dashed line (at 0.026 degrees^2) represents the signal region.

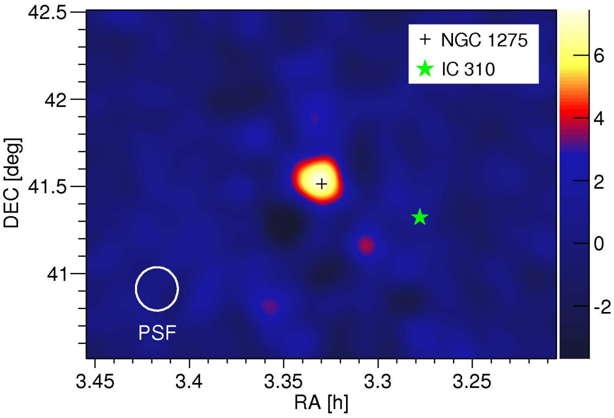

Fig. 2. Significance skymap (J2000) of the NGC 1275 region from 39.0 h of MAGIC stereo observations taken between October 2009 and February 2010, with a low energy threshold of 100 GeV. The point-spread function (PSF) of about 0.12° is also displayed.

$$\frac{\mathrm{d}F}{\mathrm{d}E} = f_0 \left(\frac{E}{100\,\mathrm{GeV}}\right)^{-\Gamma}, \tag{1}$$

with a photon index $\Gamma = 4.0 \pm 0.5_{stat} \pm 0.3_{syst}$ and a normalization constant at 100 GeV $f_0 = (5.0 \pm 0.9_{stat} \pm 1.1_{syst}) \times 10^{-10}\mathrm{cm}^{-2}\mathrm{s}^{-1}\mathrm{TeV}^{-1}$. The spectrum of Camp. 2 corresponds to the result reported in Aleksić et al. (2012a):

---

[1] The parameter θ^2 is the square angular distance between the reconstructed source of the events and the nominal positions of the expected source.

[2] The systematic errors of the flux normalization and the energy spectral slope considered here have been estimated to be less than 23% and ±0.3, respectively, whereas the systematic uncertainty on the energy scale is 17%. These values are more conservative than those presented in Aleksić et al. (2012c), given the flux weakness and the spectral steepness of NGC 1275, as measured by MAGIC.

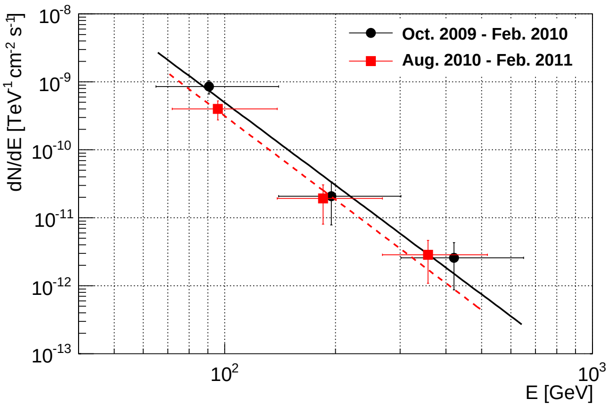

Fig. 3. NGC 1275 differential energy spectrum measured with MAGIC during two observation campaigns and their associated power-law fits. Camp. 1 data are in black with a solid line fit and Camp. 2 data are in red/grey with a dashed line fit.

$f_0 = (3.1 \pm 1.0_{stat} \pm 0.7_{syst}) \times 10^{-10}\mathrm{cm}^{-2}\mathrm{s}^{-1}\mathrm{TeV}^{-1}$ and $\Gamma = 4.1 \pm 0.7_{stat} \pm 0.3_{syst}$. One may notice that the energy range of the Camp. 1 spectrum is slightly larger than Camp. 2. This arises because the Camp. 1 spectrum must have slightly larger bin widths in energy to fulfill the significance requirement of each bin.

The mean flux above 100 GeV during Camp. 1, $(1.6 \pm 0.3_{stat} \pm 0.3_{syst}) \times 10^{-11}$ cm^{-2} s^{-1}, corresponds to about 3% of the Crab nebula flux. It is slightly higher than Camp. 2 results, $(1.3 \pm 0.2_{stat} \pm 0.3_{syst}) \times 10^{-11}$ cm^{-2} s^{-1}, but both campaigns agree within the uncertainties. No indication of spectral index variability has been found between the two campaigns. The monthly light curve (LC) of NGC 1275 above 100 GeV is shown in the top panel of Fig. 4. While the Camp. 2 LC is quite consistent with a constant flux ($\chi^2/n_{dof} = 7.4/4$, probability = 0.29), a hint of variability can be derived for the first campaign. Indeed, fitting the Camp. 1 LC with a constant flux yields a $\chi^2/n_{dof} = 22.9/4$ (probability = 1.3×10^{-4}), corresponding to a significance for a monthly variable emission of 3.6 σ.

2.2. *Fermi*-LAT

The Large Area Telescope (LAT) is a pair conversion telescope, on board the *Fermi γ-ray Space Telescope*, designed to cover the energy band from 20 MeV to greater than 300 GeV (Atwood et al. 2009). The observations used here comprise all scientific data obtained between August 4, 2008 and February 21, 2011. We have applied a zenith angle cut of 100° to greatly reduce γ-rays from the Earth's limb. The same zenith cut is also accounted for in the exposure calculation using the LAT Science Tool gtltcube. We have used the "Source" class events (Ackermann et al. 2012) which is the recommended class for regular analysis. In our analysis, Science Tools version v9r27p1 and instrumental response functions P7SOURCE_V6 were used. The lower energy bound was set at 100 MeV and the region of interest (ROI) radius at 10° (see Abdo et al. 2009). All the nearby sources in the 2FGL catalog (Nolan et al. 2012) were included in the model of the ROI, fixing their spectral index and letting their normalization free in the fit. Since no variability is expected for the underlying background diffuse emission, we fixed the normalization of both Galactic and extragalactic diffuse backgrounds to the average values determined from the whole observing period described in this paper (from August 4, 2008 to February 21, 2011). The early portion of the data between August 4, 2008 and August 13, 2009 coincides with the early LAT observations of NGC 1275 presented in Kataoka et al. (2010) (see also Brown & Adams 2011). The systematic uncertainties on the flux were estimated as 10% at 100 MeV, decreasing to 5% at 560 MeV, and increasing to 10% at 10 GeV and above (Ackermann et al. 2012).

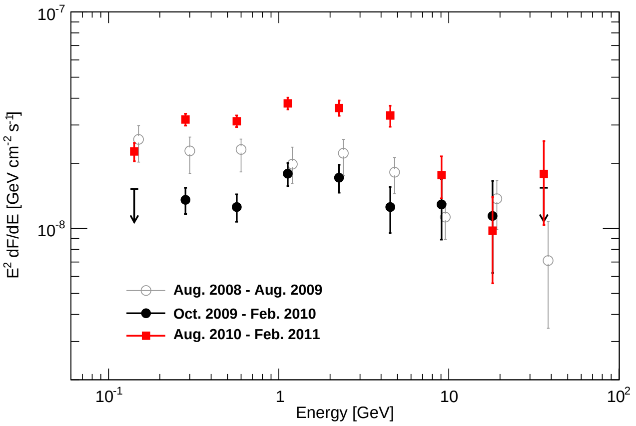

Fig. 5. NGC 1275 SED measured with *Fermi*-LAT during several periods corresponding to the first year of operation (empty circles, Kataoka et al. 2010), the first MAGIC campaign (full circles and black arrows) and the second MAGIC campaign (full squares).

The Panel (b) of Fig. 4 shows the γ-ray flux above 100 MeV of NGC 1275 from September 25, 2009 to February 18, 2011 binned at one week intervals. In each bin, the significance of the NGC 1275 detection is above the test statistic TS>10 and the ratio of flux error to flux is below 0.5 (δF/F $\lesssim$ 0.5, see Nolan et al. 2012). One can note a general trend of increasing flux towards the end of the observations, and several episodes of large flares as fast as one-week time scale.

Fig. 5 shows the *Fermi*-LAT spectral energy distributions (SED) derived for the two MAGIC-observation campaigns (MJD 55123–55241 for Camp. 1 and MJD 55417–55595 for Camp. 2) as compared with that obtained for the first year given in Kataoka et al. (2010). The spectra were obtained from nine independent energy bins: (0.1–0.2, 0.2–0.4, 0.4–0.8, 0.8–1.6, 1.6-3.2, 3.2–6.4, 6.4–12.8, 12.8–25.6, 25.6–51.2) GeV. The general spectral shape can be approximated by a power-law function with a photon index $\Gamma \simeq 2$, slightly curving down toward the highest energies. Substantial spectral evolution can be seen in different observational periods, both in the flux and peak frequencies of the γ-ray emissions. The Camp. 2 mean GeV flux is about twice as high as during the first MAGIC campaign, and the Camp. 2 SED shows a clear curvature peaking around 1 GeV, whereas the first-year SED is constantly decreasing with energy. However, above a few GeV all the spectra reach similar fluxes. The γ-ray flux seems more variable at low energy. The precise fit characterization of the LAT spectrum is discussed together with the MAGIC data in Section 3.3.

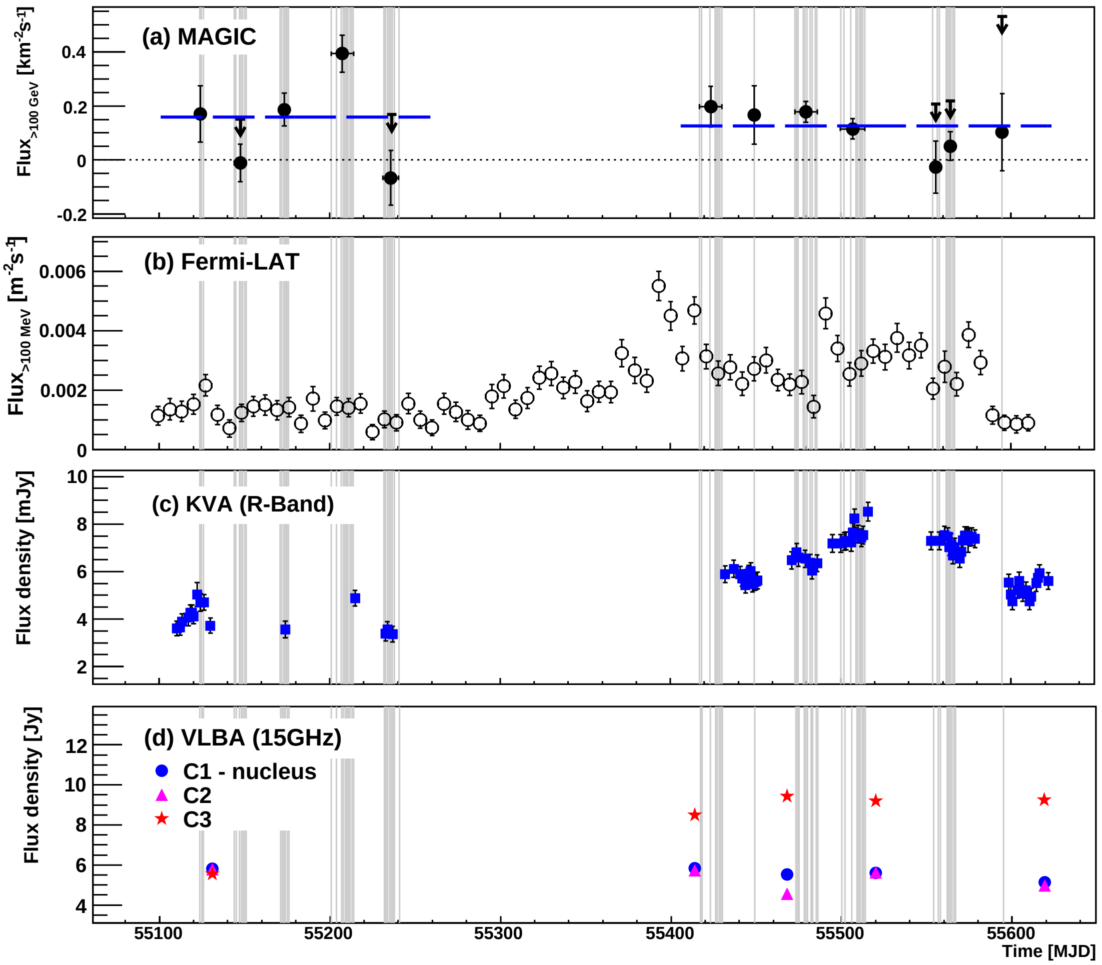

Fig. 4. Multi-frequency light curves of NGC 1275 from October 2009 to February 2011. The vertical grey lines show the exact observation dates with MAGIC. (a) The MAGIC LC above 100 GeV in monthly bins. The thick dashed lines represent the constant fit for both observation campaigns. For data showing an excess $<1\,\sigma$, upper limits (black arrows) are calculated assuming a spectral index Γ=4.0, using the Rolke et al. 2005 method with a confidence level of 95% and a total systematic uncertainty of 30%. (b) The *Fermi*-LAT LC above 100 MeV has a weekly binning. (c) The KVA R-band LC shows the core continuum flux corrected for Galactic extinction. The constant systematic error (±0.6 mJy) induced by the host-galaxy and emission-line subtraction is not included in the error bars. (d) The VLBA LCs show the 15 GHz emission from the three innermost components of the radio jet.

2.3. Chandra X-ray Observatory

The ACIS detector aboard the *Chandra X-ray Observatory* is a spectrometer with very good angular resolution ($\sim$0.5$''$) operating in the range of 0.2–10 keV. In the public archive, we found seven observations performed during the MAGIC observing period (namely ObsId 11713, 11714, 11715, 12025, 12033, 12036, 12037, PI Fabian). In NGC 1275, the nuclear X-ray flux is high enough that pileup is potentially a severe problem. For an on-axis observation, PIMMS estimates a total pileup fraction of about 52% (i.e. more than half of the incident photons are either combined into piled events or removed because their energy is higher than the spacecraft threshold). The nucleus was not the primary target of these observations and no observing strategy for minimizing nuclear pileup was actuated (e.g. selecting a subarray to reduce the nominal frame integration time, etc.). However, this set of observations was centred several arcminutes away from the nucleus (3.2$'$–7.6$'$), and this reduces the pileup because at larger offset the effective area of the mirrors is lower and the point-spread function (PSF) is larger. We simultaneously fit the three observations with offset angles $>$7.5$'$ (ObsId 12025, 12033, 12036) adopting a pileup model to correct for this effect.

We applied the standard data reduction procedure[3] using the *Chandra* Interactive Analysis of Observations CIAO 4.4, with *Chandra* Calibration Database CAL-DB version 4.4.1. We generated a new level = 2 event file applying the standard grade, status, and good time filters. We rebinned the spectrum using a 25-count threshold and fitted the spectrum in the range 0.5–9.5 keV. The three spectra were fitted simultaneously adopting the model $pileup \times phabs(mekal + zphabs(powerlaw))$ in XSPEC version: 12.7.1. where *mekal* models the thermal and line emissions of the hot diffuse gas, and *powerlaw* is the non-thermal power-law emission from the jet. The metal abundance and hydrogen density of *mekal* were fixed to 0.7 solar value and 0.1 cm^{-3} respectively. The temperature and normalization are obtained from the fit ($kT = 0.30 \pm 0.01$ keV). For the absorption, we fixed the hydrogen column den-

---

[3] http://cxc.harvard.edu/ciao/guides/acis_data.html

sity from the Galaxy ($N_{H,gal}$=1.5×10^{21} cm^{-2}) and let free the internal absorption (zN_H=5.6±0.2×10^{21} cm^{-2}). The power-law slope Γ is strongly affected by the pileup effect, so we decided to fix it in the model. All the parameters of the power-law and *mekal* model were linked together except the normalization. Table 1 provides the results of the fit for several power-law slope assumptions.

Table 1. Unabsorbed integral flux of the NGC 1275 non-thermal power-law core emission in the range 2-10 keV obtained from *Chandra* observations assuming different power-law slopes.

ObsId	Date	Γ	fit χ^2 (d.o.f.)	F(2-10 keV)^a
12025	2009-11-25	2.5	1616.8 (1075)	$1.26^{+0.1}_{-0.1}$
12033	2009-11-27			$1.27^{+0.1}_{-0.1}$
12036	2009-12-02			$1.35^{+0.1}_{-0.1}$
12025	2009-11-25	2.0	1307.4 (1075)	$1.50^{+0.1}_{-0.1}$
12033	2009-11-27			$1.49^{+0.5}_{-0.1}$
12036	2009-12-02			$1.71^{+0.4}_{-0.2}$
12025	2009-11-25	1.7	1392.8 (1075)	$2.20^{+0.3}_{-0.3}$
12033	2009-11-27			$4.40^{+1.2}_{-0.3}$
12036	2009-12-02			$5.60^{+0.1}_{-0.2}$

$^{(a)}$ Integral flux in 10^{-11} erg cm^{-2} s^{-1} (uncertainties at $\pm1\sigma$)

2.4. KVA and NOT

NGC 1275 has been monitored in the optical R-band by the Tuorla blazar monitoring programme[4] since the autumn of 2009. The observations are performed using the KVA 35 cm telescope located at La Palma. The data were reduced using the standard data analysis pipeline and the magnitudes were measured with differential photometry with an aperture of 5.0″ and the comparison stars from Fiorucci et al. (1998). The observed magnitudes varied between 13.05 and 13.3. The magnitudes are converted to flux using the standard formula $S = S_0 \cdot 10^{-mag/2.5}$ and $S_0 = 3080$ Jy.

For the calculation of the intrinsic emission from the core, the measured magnitudes over the MAGIC observing periods have to be averaged, the host galaxy subtracted, and the resulting data de-reddened. Additionally, the core flux is contaminated by emission lines which must also be subtracted. In order to estimate the contributions of the host galaxy and the emission lines to the raw KVA measurements, NGC 1275 was observed with the Nordic Optical Telescope (NOT) on November 15, 2011 using the ALFOSC instrument. Five 60 s R-band exposures and two spectra using grism 4 and slit 1″ were obtained. The images were reduced and combined using the standard IRAF tasks. The methodology of Nilsson et al. (2007) was used to estimate the contribution of the host galaxy. In short, the method is based on fitting a two-dimensional nucleus plus host galaxy model to the image and convolving the model with the PSF derived from the stars in the same field of view. The resulting host galaxy flux based on the aperture used is 11.08 ± 0.55 mJy. The line contamination is estimated from the spectrum of NGC 1275 by integrating the observed line flux within the NOT R-band filter. We find that the line contamination in the R-band is 0.9 mJy, i.e. only ∼10% of the host flux. The host and line contaminations are then subtracted to derive the core continuum non-thermal flux, which is then corrected for Galactic extinction (de-reddened) using the extinction value from Schlegel et al. (1998). The measured fluxes are shown together with the multi-frequency light curves (Fig. 4). The mean fluxes over the two MAGIC campaigns are (4.1±0.6) mJy for Camp. 1 and (6.5±0.6) mJy for Camp. 2.

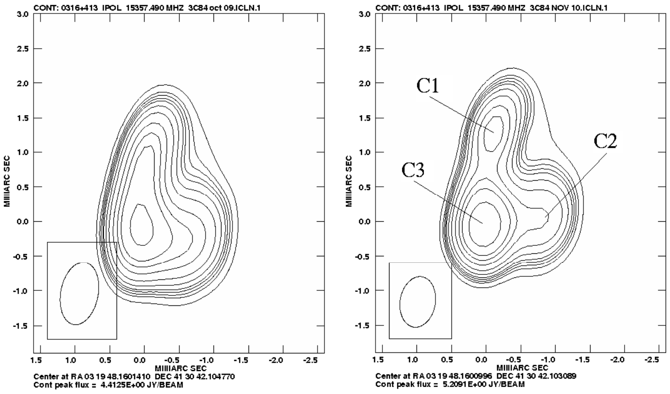

Fig. 6. MOJAVE images of 3C 84 at 15 GHz in October 2009 (left) and November 2010 (right). The contours are plotted at levels of (0.5, 0.7, 0.8, 0.9, 1, 1.2, 1.5, 2, 2.5, 3, 4) Jy/beam. The labels C1, C2 and C3 show the three bright components in the central region. The insets show the shape of the PSF.

2.5. MOJAVE observations

The Very Long Baseline Array (VLBA) is a radio interferometer using ten 25 m-diameter antennas located across the USA between Hawaii and the Virgin Islands. Thanks to its very long baselines (up to 8600 km), angular resolutions down to milli-arcseconds (mas) can be achieved. The Monitoring Of Jets in AGNs with VLBA Experiments (MOJAVE) programme is constantly observing a set of bright AGNs in the northern hemisphere at 15 GHz (Lister et al. 2009).

The calibrated data of the MOJAVE programme have been reduced using the NRAO Astronomical Imaging Processing System (AIPS). In this work, we analyzed five epochs covering the time interval from October 2009 to February 2011. Fig. 6 shows the total intensity images of the central region (∼1 pc) at 15 GHz, featuring three bright components C1, C2 and C3. Generally C1 is understood as being the nuclear core emission. C3 corresponds to the rapidly growing component that recently appeared (Nagai et al. 2010). The position and flux density for each component was derived by means of the task JMFIT, which fits a Gaussian function to a selected area in the image plane. The obtained flux densities are listed in Table 2 and shown in Panel (d) of Fig. 4. We consider the VLBA accuracy of amplitude calibration as the dominant uncertainty (at the level of 5%). While the flux densities of C1 and C2 do not show considerable variability, the intensity of C3 significantly increases between the beginning and the end of the observational campaign (as reported Table 2).

---

[4] http://users.utu.fi/kani/1m

Table 2. Flux densities of the components C1, C2 and C3 obtained from MOJAVE data at 15 GHz.

Epoch	C1 (Jy)	C2 (Jy)	C3 (Jy)
2009-10-09	5.80 ± 0.29	5.79 ± 0.29	5.54 ± 0.27
2010-08-06	5.84 ± 0.29	5.74 ± 0.29	8.50 ± 0.43
2010-09-29	5.48 ± 0.27	4.53 ± 0.23	9.42 ± 0.47
2010-11-20	5.59 ± 0.28	5.62 ± 0.28	9.20 ± 0.46
2011-02-27	5.13 ± 0.26	4.97 ± 0.25	9.21 ± 0.46

2.6. Other multi-frequency data

NGC 1275 is a famous and bright object that is regularly observed at many frequencies. Some observations made during the period of interest here (October 2009 – February 2011) were reported in scientific journals and can be used for our broadband study without a dedicated data processing.

NGC 1275 was part of the Early Release Compact Source Catalogue of the *Planck* microwave observatory (*Planck* Collaboration 2011, and references therein). This catalogue contains NGC 1275 observations taken during two periods: from August 29 to September 4, 2009 and from February 10 to 19, 2010. Both periods are close to the first MAGIC observation campaign. More recent *Planck* observations taken from August 29 to September 4, 2010, corresponding to the second MAGIC campaign, are reported in Giommi et al. (2012). The derived spectrum between 30 GHz and 857 GHz is in good agreement with the one reported in the Early Release Compact Source Catalogue between 30 GHz and 353 GHz. The microwave flux of NGC 1275 was quite stable during the MAGIC observations.

Giommi et al. (2012) also reported contemporaneous observations in the ultraviolet (UV)/optical band (170–650 nm) with *Swift*-UVOT taken August 9, 2010 at the beginning of the second MAGIC campaign.

In radio, NGC 1275 was regularly monitored with the Metsähovi 14 m single-dish telescope with additional VLBI observations of the VERA stations at 43 GHz (Nagai et al. 2012a) and the MOJAVE programme at 15 GHz (already discussed in Section 2.5). Moreover, the GENJI programme (Nagai et al. 2012b) started a dense VLBI monitoring of NGC 1275 at 22 GHz in November 2010 (during the second MAGIC observation campaign). All radio data show the same trend of a slowly increasing flux with time from the component C3 during the period of interest.

3. Interpretations

3.1. Data contamination

The majority of known VHE γ-ray emitting AGNs are blazars, i.e. with a jet pointing directly to the observer. In such cases, the non-thermal jet emission is highly boosted and predominates over other components. It is rather simple to subtract the background emission from the host galaxy. For NGC 1275, however, this is much more difficult. Thermal and non-thermal radiations can be emitted by extended structures in the host galaxy or even the host cluster of galaxies. Thus, observations with different angular resolution can integrate signal from different regions.

While the rapid and strong variability measured by *Fermi*-LAT implies that the γ-ray emission is largely dominated by a compact source likely close to the nucleus, there are strong indications that at other frequencies other emitting components contribute significantly to the observed flux. In optical, the KVA measurements have been corrected for both the host-galaxy and emission-line contributions. They are still significantly higher than previous *Hubble Space Telescope* (*HST*) measurements taken in 1994–1995 (Chiaberge et al. 1999; Baldi et al. 2010) when the radio core emission was similar to its level in 2009–2011 (see Effelsberg light curve in Nagai et al. 2010). The HST observations are characterized by an extremely good angular resolution allowing the emission to be pinpointed from the innermost regions of the jet. The small discrepancy between our measurement and the *HST* results could be explained by temporal variability but also by the limited angular resolution of KVA, which may contain large-scale jet contributions. In radio, VLBA provides an extremely good angular resolution which allows us to resolve three components in the sub-parsec core region. However, this resolution ($\sim$0.2 pc) is still much larger than the γ-ray emission region size expected from the week-scale variability ($\sim$0.01 pc). Substructures not resolved by VLBA can therefore exist. *Planck* and UVOT both have relatively broad angular resolution and their measurements are most likely contaminated by large-scale emission. Thus our results from radio to X-rays should be considered firstly as upper limits of the low energy counterpart of the γ-ray emitting region.

3.2. Optical γ-ray correlation

We measured flux variability at different energy bands (Fig. 4). The light curves for GeV γ-rays, optical and the C3 radio component all show a similar trend. The intense monitoring in optical and GeV γ-rays allows us to more deeply study this correlation. For every time bin of the *Fermi*-LAT weekly LC containing simultaneous KVA observations, we calculated the mean optical flux density of the core. Fig. 7 shows the γ-ray flux above 100 MeV as a function of the optical core emission for the 23 independent weeks with simultaneous *Fermi*-LAT and KVA observations. A clear correlation is visible. The linear correlation coefficient (Bravais-Pearson coefficient) is $0.79^{+0.07}_{-0.10}$. The correlation can also be characterized using the prescription of Edelson & Krolik (1988), which, unlike the Pearson coefficient calculation, takes into account the measurement uncertainties. This leads to a discrete correlation function DCF = 0.86±0.21. Both statistical procedures to quantify the optical γ-ray correlation lead to the same conclusion: a positive correlation at the level of 4–5 σ.

This correlation strongly suggests that the corrected KVA results are dominated by the optical counterpart of the γ-ray emitting region. The lower optical level measured in 1994–1995 by *HST* (<2 mJy) is most likely due to a weaker inner jet activity which, indeed, was not detected in γ-rays with *CGRO*-EGRET during this period.

Different types of correlation can be expected depending on the emission model and on the physical parameter driving the flux variation. In a simple SSC model (see description Section 3.4), the variation of the electron density implies a quadratic correlation whereas the magnetic field variation implies a linear correlation. We fit the data assuming correlation functions of the form $F_\gamma = \alpha(F_{opt})^\beta$.

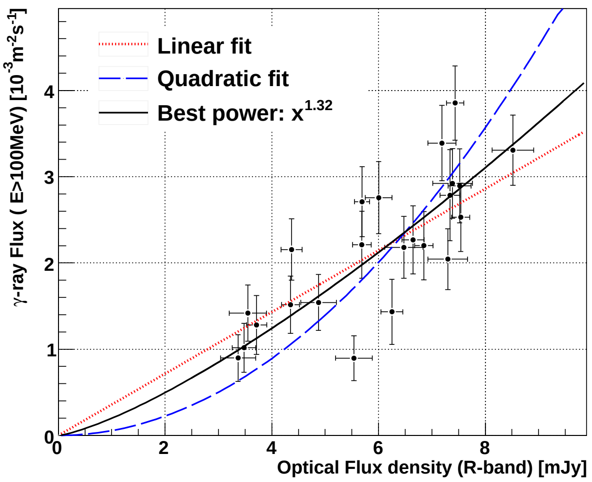

Fig. 7. NGC 1275 γ-ray flux above 100 MeV (*Fermi*-LAT) as a function of the optical continuum core flux density (KVA). The dotted and dashed lines represent the linear and quadratic fit respectively. The solid line is the best fit with a free correlation factor ($F_\gamma = \alpha(F_{opt})^\beta$ with β=1.32).

The best fit is obtained for β=1.32 but both a linear (β=1) and a quadratic (β=2) correlation can fit the data as well.

3.3. Fit of γ-ray SED

The photon indices of the energy spectrum measured quasi-simultaneously with *Fermi*-LAT ($\Gamma \simeq$2) and MAGIC ($\Gamma \simeq$4) are very different. Fig. 8 shows the SED between 100 MeV and 650 GeV corresponding to the two observation campaigns. We fit several functions to these SEDs taking into account only the statistical errors of each data point. Table 3 gives the functional forms used and the fit results.

Table 3. Parameters of the NGC 1275 γ-ray SED fit over the energy range 0.1 – 650 GeV, for different fit functions:

power law: $dF/dE = f_0(\frac{E}{GeV})^{-\Gamma}$

Epoch	$f_0{}^a$	Γ	χ^2/dof	Prob.
Camp. 1	111±8	2.38±0.03	57.4/8	1.5e-9
Camp. 2	176±7	2.41±0.02	317/10	3.e-62

power law with exponential cutoff: $\frac{dF}{dE} = f_0(\frac{E}{GeV})^{-\Gamma}e^{-E/E_c}$

Epoch	$f_0{}^a$	Γ	$E_c{}^b$	χ^2/dof	Prob.
Camp. 1	149±10	1.93±0.06	67±12	8.6/7	0.28
Camp. 2	411±25	1.75±0.05	7.3±1.6	26.5/9	0.0017

power law with a sub-exp. cutoff: $\frac{dF}{dE} = f_0(\frac{E}{GeV})^{-\Gamma}e^{-\sqrt{E/E_c}}$

Epoch	$f_0{}^a$	Γ	$E_c{}^b$	χ^2/dof	Prob.
Camp. 1	201±17	1.77±0.08	13.1±4.2	9.4/7	0.22
Camp. 2	536±51	1.72±0.05	5.0±1.6	19.3/9	0.023

log parabola: $dF/dE = f_0(\frac{E}{GeV})^{-2-\beta log(E/E_p)}$

Epoch	$f_0{}^a$	β	$E_p{}^c$	χ^2/dof	Prob.
Camp. 1	163±11	0.26±0.04	2.8±1.5	12.3/7	0.09
Camp. 2	371±13	0.31±0.03	1.1±0.2	13.4/9	0.15

$^{(a)}$ Differential flux normalization in 10^{-10} GeV^{-1} cm^{-2} s^{-1}
$^{(b)}$ Cutoff energy in GeV
$^{(c)}$ Peak energy in GeV

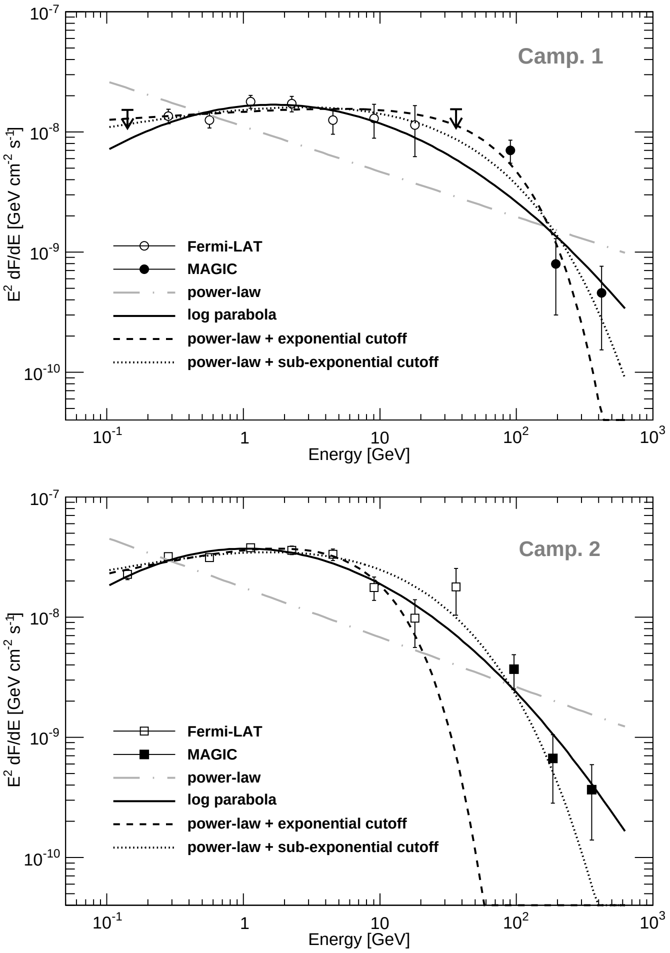

Fig. 8. NGC 1275 SED in γ-ray band measured with MAGIC and *Fermi*-LAT together with fit functions of the data (see parameters in Table 3). Upper and lower panels correspond to the periods October 2009 – February 2010 and August 2010 – February 2011 respectively.

A power-law fit is completely excluded as already suggested by previous VHE upper limits contemporaneous to *Fermi*-LAT data in 2008 (Acciari et al. 2009; Aleksić et al. 2010b). A power-law spectrum with an exponential cutoff fits well the first campaign but does not match the second one where the LAT data clearly show a curvature. Assuming a less sharp cutoff (a power-law with a sub-exponential cutoff), one can fit both campaigns quite well. This gives a photon index of $\Gamma \simeq 1.75$ at low energy which matches well the non-thermal power-law component seen in X-ray by *Chandra* (Balmaverde et al. 2006) and *Swift*/BAT (Ajello et al. 2009). As explained in Acciari et al. (2009), this function corresponds to the γ-ray spectral shape expected for the inverse Compton emission of an electron population with an energy distribution following a power law with an exponential cutoff at high energy[5].

---

[5] Strictly, a sub-exponential description for the cut-off of the inverse Compton spectrum is valid only in the Thomson regime. As discussed in Section 3.4, the scattering responsible for emission at the high-energy peak in NGC 1275 mainly occurs in the Klein-Nishina regime. In this case, that particular shape can still be used as an approximation.

Finally, a curved power-law (log parabola) provides the best fit for Camp. 2 data and a reasonably good fit for Camp. 1. It allows us to determine the peak energy of the SED, which varies marginally from 2.8±1.5 GeV (Camp. 1) to 1.1±0.2 GeV (Camp. 2).

3.4. Broadband SED and emission models

Nearly simultaneous SEDs for Camp. 1 and Camp. 2, assembled with the data described in the previous section, are reported in Fig. 9 (red symbols) and Fig. 10 (blue symbols) respectively. The non-thermal X-ray component spectra from Balmaverde et al. (2006) (*Chandra*) and Ajello et al. (2009) (*Swift*/BAT), as well as the optical-IR measurement by *HST* (Chiaberge et al. 1999; Baldi et al. 2010) are also reported (green symbols).

The data hint for a double-peaked SED, similar to the other TeV emitting AGNs. The similarity of this SED with that of blazars is a clear indication that the broadband emission arises in the relativistic jet. The available data provide an excellent description of the high-energy bump of the SED. In particular, it is possible to constrain the position of the peak with good accuracy. On the other hand, the low energy bump is poorly constrained by our radio to UV simultaneous data, which are more likely dominated by larger scale emission regions. The correlation between the optical and the γ-ray LC suggests that the non-thermal continuum from the NGC 1275 nucleus is dominated by the emission from the same region. We assume that the low-energy component of this region is at the level of our KVA measurements corrected for the host-galaxy and line emissions.

For our model, we assume, as a starting point, that the emission is coming from a unique uniform spherical region (a bulk plasma) moving along the jet. We reproduce the SED using a synchrotron self-Compton (SSC) model (for details see Maraschi & Tavecchio 2003) considering an electron-density energy distribution of the form $N(\gamma) = K\gamma^{-n}\exp(-\gamma/\gamma_{\rm c})$, with a Lorentz factor $\gamma > \gamma_{\rm min}$. Such a very simple distribution is naturally expected in the case of Fermi-I type shock acceleration (e.g. Blandford & Eichler 1987) and it is also supported by the γ-ray SED fits of Section 3.3. The other physical parameters specifying the model are the intensity of the (assumed tangled) magnetic field, B, the source radius, R, and the Doppler factor, δ. The latter parameter is given by $\delta = 1/[\Gamma_b(1-\beta_b\cos\theta_{\rm v})]$, where β_b is bulk speed of the plasma, Γ_b is the bulk Lorentz factor, $\Gamma_b = [1-\beta_b^2]^{-1/2}$, and $\theta_{\rm v}$ is the angle between the bulk velocity and the line of sight. Our model has then only seven independent parameters (K, n, $\gamma_{\rm min}$, $\gamma_{\rm c}$, B, R, and δ).

Following the radio counter-jet evidence (Vermeulen et al. 1994; Walker et al. 1994; Asada et al. 2006), we first assume an observing angle $\theta_{\rm v} = 30°$, which is the lowest angle compatible with the radio observations. The maximum value of the Doppler factor allowed is then $\delta = 2$ reached for a bulk Lorentz factor $\Gamma_b = 2$. Having fixed the Doppler factor, the source size can be constrained by the observed variability timescale in the *Fermi*-LAT band, $t_{\rm var} \simeq 1$ week, which limits the radius through the causality relation $R < ct_{\rm var}\delta \simeq 4\times10^{16}$ cm, rather similar to the sizes used in most blazar models. During Camp. 1 the *Fermi*-LAT LC is smoother and the constraint on the radius must be relaxed to light-month scales: $R/\delta < 10^{17}$ cm.

Some estimates of the other physical parameters can be derived with simple arguments. While the peak of the SSC bump arises from scattering in the Klein-Nishina (KN) regime, its frequency can be directly used to estimate the Lorentz factor $\gamma_{\rm c}$ of the electrons at the high energy cutoff. Following Tavecchio et al. (1998)[6], the frequency of the SSC peak, $\nu_{\rm SSC}$, is given as $h\nu_{\rm SSC} \simeq m_e c^2\,\gamma_{\rm c}\,g(\alpha)\delta$, where $g(\alpha) = \exp[1/(\alpha-1)]$ is a function of the energy-flux spectral slope of the rising edge of the synchrotron and inverse Compton bumps, $\alpha = (n-1)/2$. The fit of the SSC bump with a power-law with a sub-exponential cutoff, reported in Section 3.3, provides a good estimation of the rising edge slope $\alpha \simeq 0.75 \pm 0.1$ (The fit parameter Γ is the power-law index of the photon flux, $\Gamma = \alpha + 1.$). This value is also in a good agreement with the spectral slope measured in hard X-rays with *Swift*-BAT ($\alpha = 0.7^{+0.3}_{-0.7}$, Ajello et al. 2009). For $\alpha = 0.75$, the value of $g \simeq 0.02$. The SSC peak is measured around $\nu_{\rm SSC} \simeq 10^{24}$ Hz, implying $\gamma_c \simeq 2\times10^5$. The frequency of the synchrotron peak, $\nu_{\rm s}$ is now found as: $\nu_{\rm s} \simeq 2.8\times10^6 B\gamma_{\rm c}^2\delta$ Hz. The condition (Tavecchio et al. 1998) that the SSC peak is produced by scatterings in the KN regime is $h\gamma_{\rm c}\nu_{\rm s}/\delta > m_e c^2$, which, after some operations, can be expressed as a limit for the magnetic field, $B > B_{\rm cr}\gamma_{\rm c}^{-3}$ G, where $B_{\rm cr} = 4.4\times10^{13}$ G is the critical magnetic field. Inserting the value above for $\gamma_{\rm c}$ we found $B > 4\times10^{-3}$ G.

An estimate of the magnetic field can be derived from the ratio between the synchrotron and SSC luminosities, $L_{\rm s}/L_{\rm SSC} \simeq U_B/U_{\rm rad}$ where $U_B = B^2/8\pi$ is the magnetic energy density and $U_{\rm rad}$ is the synchrotron radiation energy density (Tavecchio et al. 1998). The latter can be calculated from $U_{\rm rad} \simeq L_{\rm s}/(4\pi R^2 c\delta^4)$. Assuming the SSC emission occurs in the KN regime reduces the radiation energy density available for the emission. However in first approximation one can neglect this effect (such derived value is formally a lower limit of the magnetic field). Finally, the magnetic field can be expressed as $B \simeq (2/c)^{1/2}R^{-1}\delta^{-2}L_{\rm s}\,L_{\rm SSC}^{-1/2}$. Deriving the luminosities from the SED and using $R = 4\times10^{16}$ cm, we obtain $B \simeq 0.1$ G. This value is well above the limit for the KN regime calculated above, confirming the previous assumption.

Table 4 reports the parameters obtained for the emission model, shown as dashed curves in Figs. 9-10. The frequency of the synchrotron peak is relatively high ($>10^{16}$ Hz) and the model predicts soft X-ray emission dominated by the end of the synchrotron hump. The expected X-ray flux is much higher than the archival *Chandra* data and shows a very different spectral shape. However, our model for Camp. 1 is in good agreement with the simultaneous *Chandra* data analyzed in section 2.3, if one assumes a photon index Γ=2.5 as expected by our model. Unfortunately, the quality of these data, strongly affected by pileup, does not allow us to derive better constraints. For Camp. 2, the expected X-ray flux is higher and the UV emission reaches almost the *Swift*-UVOT data. The simultaneous data do not rule out our model but the overall shape with a syn-

---

[6] Tavecchio et al. (1998) consider an electron energy distribution with a broken power-law shape. The results can be extended to the present case of a power law with exponential cutoff by identifying the break parameter γ_b with cutoff parameter γ_c and taking the limit $\alpha_1 = \alpha$ and $\alpha_2 \gg 1$.

	δ	B [mG]	K [10^4 cm^{-3}]	R [10^{16} cm]	$\gamma_{\rm min}$	$\gamma_{\rm c}$	n
Camp. 1	4	42	20	7.9	100	2.2×10^5	2.55
	2	170	18	8.2	100	3.5×10^5	2.55
Camp. 2	4	38	9	8.2	100	0.9×10^5	2.4
	2	380	14.7	4.1	100	1.5×10^5	2.4

Table 4. Parameters for the models reported in Figs. 9-10. For both epochs the Table reports the result obtained for two different choices of Doppler factor, $\delta = 2$ and 4. The parameters are the magnetic field B, the particle density K, the source radius R, the minimum electron Lorentz factor, $\gamma_{\rm min}$, the cut-off Lorentz factor $\gamma_{\rm c}$, and the electron spectrum slope n.

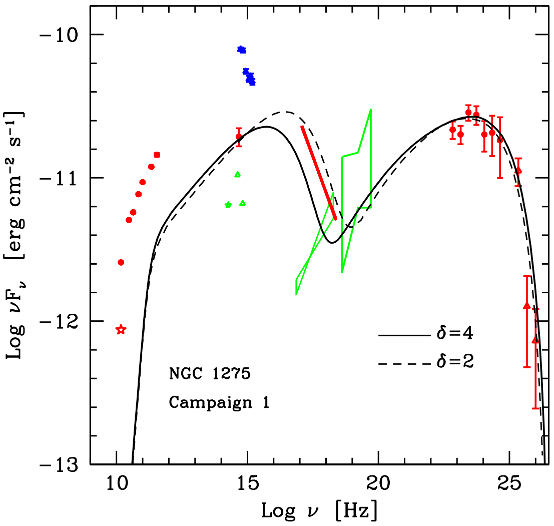

Fig. 9. NGC 1275 SED for the epoch of Camp. 1 (October 2009 – February 2010). Red symbols show nearly simultaneous data from MOJAVE, KVA, *Chandra* (when assuming a power-law slope Γ=2.5), *Fermi*-LAT and MAGIC analyzed in this paper. Contemporaneous *Planck* data from *Planck* Collaboration (2011) are also shown in red. The red star in radio shows the level of the individual sub-parsec components (C1, C2 and C3 have nearly the same flux). Green bow-ties in the X-ray band report the archival *Chandra* and *Swift*-BAT results from Balmaverde et al. (2006) and Ajello et al. (2009), respectively. Green symbols report optical-IR measurement by *HST* from Chiaberge et al. (1999) (triangles) and Baldi et al. (2010) (star). The blue points show the August 2010 *Swift*-UVOT data from Giommi et al. (2012) (host galaxy contribution corrected). The dashed and solid lines report the SSC models for $\delta = 2$ ($\theta_v < 30°$) and $\delta = 4$ ($\theta_v < 15°$) respectively.

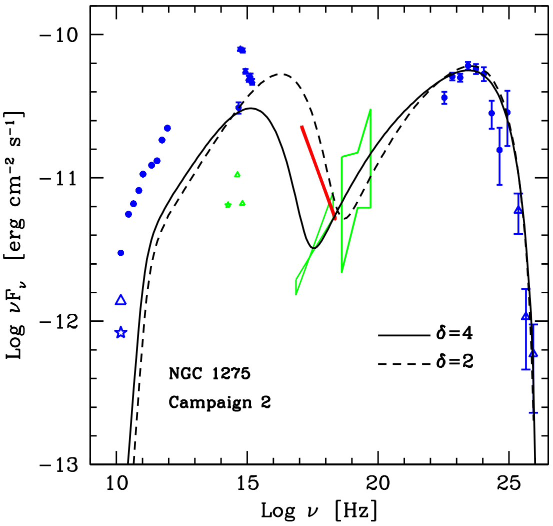

Fig. 10. NGC 1275 SED for the epoch of Camp. 2 (August 2010 – February 2011). Symbols as in Fig. 9. Blue symbols show nearly simultaneous data from MOJAVE, KVA, *Fermi*-LAT and MAGIC analyzed here, and contemporaneous *Swift*-UVOT and *Planck* data from Giommi et al. (2012). In radio, the level of the sub-parsec components C1 (blue star) and C3 (blue triangle) are also shown.

chrotron peak in X-ray seems unlikely. The X-ray flux has never been measured at such a high level. A lower synchrotron peak frequency would be more natural.

As discussed in Tavecchio & Ghisellini (2008) and Aleksić et al. (2010b) a small "distance" between the SED peaks is unavoidable for low Doppler factors. In order to increase the separation between the peaks, shifting the synchrotron bump to lower frequencies, we are forced to increase δ. In fact, using the relations developed above it is relatively easy to see that (for a fixed $\nu_{\rm SSC}$) the synchrotron peak frequency is related to the corresponding Doppler factor by $\nu_{\rm s} \propto \delta^{-4}$. In Figs. 9-10 and Table 4, we also report the models for a Doppler factor twice as large, $\delta = 4$ (solid lines). According to the scaling above, the synchrotron peak frequency decreases by more than a decade. The optical flux stays at the same level, while the UV and X-ray emission decrease significantly. Such a value of the Doppler factor is however disfavored, since it requires an angle between the plasma bulk velocity and the line of sight smaller than 15°.

4. Discussion

The overall SED of NGC 1275 suggests blazar-like emission. A one-zone SSC model can fit the data assuming a jet viewing angle ($\theta_{\rm v} = 30°$) compatible with the radio observation. All parameters (with possibly the exception of the bulk Lorentz factor Γ_b) derived from this modeling are in the range of the values typically obtained for VHE γ-ray emitting BL Lac objects (e.g., Tavecchio et al. 2010). Another interesting remark concerns the required slope of the electron energy distribution, close to 2.5. This value is in good agreement with recent simulations by Sironi & Spitkovsky (2011) who showed that, for low values of the jet magnetization (such as those derived by our SED modeling) Fermi-I shock acceleration proceeds efficiently, leading to power-law tails with slope $n = 2.5$.

All these elements support the view that the γ-ray emission of NGC 1275 comes from a misaligned BL Lac jet, as for the other VHE γ-ray emitting radio galaxies, and consistent with the unification scheme (e.g., Urry & Padovani 1995). A notable exception, however, is the bulk Lorentz factor, constrained to have a rather low value ($\Gamma_b \simeq 2$) as compared to the typical $\Gamma_b > 10$ inferred in BL Lacs. Indeed, with a jet viewing angle $\theta_{\rm v} \simeq 30°$, a larger Γ_b would imply a smaller Doppler factor while our model with $\delta = 2$ already seems at the lower edge of the acceptable range (a lower δ would imply a smaller distance between the two SED peaks, inducing a too high X-ray flux). Such a low Γ_b would indicate either that the jet of NGC 1275 is ejected at a lower speed than in blazars or that the jet suffers strong acceleration/deceleration in the vicinity of the central engine. The kinematics of the radio knots might suggest acceleration along the NGC 1275 jet (Dhawan et al. 1998). Its γ-ray emitting region could then be closer to the central black hole than for typical blazars (before the bulk is accelerated to its full speed).

However, a larger bulk Lorentz factor would be possible with smaller jet sight angle $\theta_{\rm v}$. For example, a bulk emitting region with $\Gamma_b = 10$, would be seen with a Doppler factor $\delta = 2$ for $\theta_{\rm v} = 17°$ and with $\delta = 4$ for $\theta_{\rm v} = 12°$. In the past, a smaller viewing angle has been suggested for the innermost jet (Krichbaum et al. 1992; Veron 1978). The NGC 1275 core could be then a BL Lac with strong jet bending at larger scale. The high energy non-thermal continuum of NGC 1275 could be also dominated by a substructure of the jet pointing closer to our direction than the overall radio jet. Such scenarios have been already proposed to explain the γ-ray emission from other TeV radio galaxies (M 87, Cen A). This substructure could originate from the jet formation zone near the central black-hole where the jet is less collimated (Lenain et al. 2008) or from mini-jets in the main jet induced by magnetic reconnections (Giannios et al. 2010; Cui et al. 2012). Alternatively, the emission can arise in a magneto-centrifugally accelerated flow (e.g., Rieger & Mannheim 2002), whose weak collimation would be compatible with the large viewing angles inferred for radio galaxies.

One may notice that our model predicts at 15 GHz a much lower flux than the VLBA measurements, even in a single substructure. This is related to the relatively high-energy peak of the synchrotron component. The radio emission could come from another, more external, region where the low-energy electrons could diffuse. The variability of such an external component should be much smoother. The similar long-term trend of the C3 component and the GeV γ-ray emission makes it a suitable candidate for hosting the γ-ray emitting region. However the apparent velocity of this component, β_{app}=0.23 (Nagai et al. 2010), is much too slow compared to the apparent velocity of the emitting region of our one-zone SSC model. For $\theta_{\rm v} = 30°$ and $\Gamma_b = 2$, the expected apparent velocity is superluminal, $\beta_{app} = \frac{\beta_b sin(\theta_{\rm v})}{1-\beta_b cos(\theta_{\rm v})} \simeq 1.7$. The models with smaller viewing angle would have even larger β_{app}. Actually, the C3 radio component and the γ-ray source may not be co-spatial but the increasing emission in both simply connected to a general increasing activity of the AGN. Moreover, no clear correlation on short timescales was found by Nagai et al. (2012a).

The difficulty to determine the correct bulk Lorentz factor of the jet is not specific to NGC 1275 but it is a general issue of the AGN unification scheme, the so-called "bulk Lorentz factor crisis" (Henri et al. 2006). While one-zone SSC models of TeV blazars require a large Lorentz factor ($\Gamma_b > 10$), geometrical beaming arguments on FR I radio galaxy - BL Lac unification predict a small value ($\Gamma_b \simeq 3$) (Chiaberge et al. 2000). More complex models, assuming, for example, a structured jet with different emission zones (Ghisellini et al. 2005) or blob speed changes along the jet (Georganopoulos & Kazanas 2003), must be developed to solve this crisis. The simultaneous broadband observations of NGC 1275 reported here provide a rare view of a likely misaligned BL Lac object. They provide new constraints on models developed to reconcile the VHE γ-ray observations and the unification scheme of AGN.

5. Summary and conclusion

We analyzed multi-frequency observations of NGC 1275 contemporaneous to two MAGIC observation campaigns carried out from October 2009 to February 2011. MAGIC data analysis, with an energy threshold of 100 GeV, resulted in the detection of the source during both campaigns separately, confirming that NGC 1275 belongs to the very restricted club of radio galaxies detected at VHE. The ~65-650 GeV spectra measured with MAGIC are very similar for both campaigns. The monthly VHE LC shows only a hint of variability ($3.6\,\sigma$) during the first campaign. *Fermi*-LAT results between 100 MeV and ~50 GeV present different features. The LAT LC shows a clear week-scale variability and the two derived spectra, corresponding to each of the MAGIC campaigns, show differences in both flux intensity and spectral shape. Nevertheless, the combined LAT/MAGIC spectra can be well fit by both a log parabola and a power law with a sub-exponential cutoff. The SED-peak energies of the log parabolic fits are 2.8±1.5 GeV (Camp. 1) and 1.1±0.2 GeV (Camp. 2). The sub-exponential cutoff energies are 13.1±4.2 GeV (Camp. 1) and 5.0±1.6 GeV (Camp. 2). The rapid variability and spectral evolution implies that the γ-ray emitting region is a compact zone in the AGN. The KVA R-band LC, corrected for host-galaxy and emission-line contaminations, shows a very similar shape as the *Fermi*-LAT LC. This almost linear correlation strongly suggests that the optical counterpart of the very compact γ-ray emitting region dominates the corrected KVA result. The 15 GHz MOJAVE data allow us to derive the LC of the three inner-most radio components. The recently born C3 component shows a similar LC trend as the KVA and LAT LCs. This makes this jet feature a possible candidate as the γ-ray emitting region.

We modeled the simultaneous broadband SED with a simple one-zone SSC emission model assuming a power-law with an exponential cutoff for the electron energy distribution. While the high energy peak is well constrained by the LAT and MAGIC data, at low energy most of our simultaneous data must be considered as upper limits due to possible contaminations. We assumed as optical flux the corrected KVA data which show correlation with the γ-ray flux. The relatively large angle between the NGC 1275 jet and the line of sight ($\theta_\mathrm{v} = 30°$–$55°$) strongly limits the Doppler factor δ. A model with $\delta = 2$ ($\theta_\mathrm{v} = 30°$ and $\Gamma_b = 2$) can fit SED of both epochs and explain the multi-frequency behavior (optical-GeV correlation and rapid variability). However, the expected X-ray level is in tension with the *Chandra* measurements and models with lower δ would hardly match the data as they would imply a too small spread between the low- and high-energy SED peaks. On the other hand, models with larger δ (such as $\delta = 4$) would fit the SED well but would require smaller θ_v. In fact, the parameters of our models are in the typical range found for BL Lacs, except for the bulk Lorentz factor. NGC 1275 could then be a misaligned BL Lac with a particularly low bulk Lorentz factor or be more aligned than we think. Assuming a smaller θ_v (10–15°), larger bulk Lorentz factors ($\Gamma_b > 10$) are possible. A γ-ray emitting region with a velocity more aligned to the line of sight than the parsec-scale radio jet could be explained by a jet bending in the innermost region, a larger jet opening angle near the central black hole, or mini-jets within the main jet. Multi-zone models would be certainly more appropriate for interpreting the NGC 1275 AGN emission and its connection to BL Lac objects.

Acknowledgements. The MAGIC collaboration would like to thank the Instituto de Astrofísica de Canarias for the excellent working conditions at the Observatorio del Roque de los Muchachos in La Palma. The support of the German BMBF and MPG, the Italian INFN, the Swiss National Fund SNF, and the Spanish MICINN is gratefully acknowledged. This work was also supported by the CPAN CSD2007-00042 and MultiDark CSD2009-00064 projects of the Spanish Consolider-Ingenio 2010 programme, by grant DO02-353 of the Bulgarian NSF, by grant 127740 of the Academy of Finland, by the DFG Cluster of Excellence "Origin and Structure of the Universe", by the DFG Collaborative Research Centers SFB823/C4 and SFB876/C3, and by the Polish MNiSzW grant 745/N-HESS-MAGIC/2010/0.

The *Fermi*-LAT Collaboration acknowledges ongoing support from a number of agencies and institutes that have supported both the development and the operation of the LAT as well as scientific data analysis. These include the National Aeronautics and Space Administration and the Department of Energy in the United States, the Commissariat à l'Energie Atomique and the Centre National de la Recherche Scientifique/Institut National de Physique Nucléaire et de Physique des Particules in France, the Agenzia Spaziale Italiana and the Istituto Nazionale di Fisica Nucleare in Italy, the Ministry of Education, Culture, Sports, Science and Technology (MEXT), High Energy Accelerator Research Organization (KEK) and Japan Aerospace Exploration Agency (JAXA) in Japan, and the K. A. Wallenberg Foundation, the Swedish Research Council, and the Swedish National Space Board in Sweden.

Additional support for science analysis during the operations phase is gratefully acknowledged from the Istituto Nazionale di Astrofisica in Italy and the Centre National d'Etudes Spatiales in France.

This research has made use of data from the MOJAVE database that is maintained by the MOJAVE team (Lister et al. 2009).

References

Abdo, A. A., et al. 2009, ApJ, 699, 31
Acciari, V. A., et al. 2009, ApJ, 706, L275
Ackermann, M., Ajello, M., Albert, A., et al. 2012, ApJS, 203, 4
Ajello, M., et al. 2009 ApJ, 690, 367
Albert, J., et al. 2008a, ApJ, 674, 1037
Albert, J., et al. 2008b, Nucl. Instrum. Meth., A594, 407
Albert, J., et al. 2008c, Nucl. Instrum. Meth., A588, 424
Aleksić, J., et al. 2010a, ApJ, 723, L207
Aleksić, J., et al. 2010b, ApJ, 710, 634
Aleksić, J., et al. 2012a, A&A, 539, L2
Aleksić, J., et al. 2012b, A&A, 541, 99
Aleksić, J., et al. 2012c, Astropart. Phys., 35, 435
Aleksić, J., et al. 2013, submitted to A&A, arXiv:1305.5147
Aliu, E., et al. 2009, Astropart. Phys., 30, 293
Asada, K., et al. 2006, Publ. Astron. Soc. Japan, 58, 261
Atwood, W. B., Abdo, A. A., Ackermann, M., et al. 2009, ApJ, 697, 1071
Baldi, R. D., Chiaberge, M., Capetti, A., et al. 2010, ApJ, 725, 2426
Balmaverde, B., Capetti A., Grandi P. et al. 2006, A&A, 451, 35
Blandford, R., & Eichler, D. 1987, Phys. Rep., 154, 1
Brown, A. M. & Adams J. 2011, Mon. Not. R. Astron. Soc., 413, 2785
Caulet, A. et al. 1992, ApJ, 388, 301
Celotti, A., & Ghisellini, G. 2008, MNRAS, 385, 283
Chiaberge, M., Capetti, A., & Celotti, A. 1999, A&A, 349, 77
Chiaberge, M., et al. 2000, A&A, 358, 104
Churazov, E., et al. 2003 ApJ, 590, 225
Conselice, C. J., et al. 2001, The Astronomical Journal, 122, 2281
Colafrancesco, S., Marchegiani P., & Giommi P. 2010, A&A, 519, 82
Cui, Y.-D. et al. 2012, ApJ, 746 177
Dhawan, V., Kellermann K. I. & Romney J. D. 1998, ApJ, 498, L111
Eckert D. & Paltini S. 2009, A&A, 495, 415
Edelson, R. A. & Krolik J. H. 1988 ApJ, 333, 646
Fabian, A. C., et al. 2011, Mon. Not. R. Astron. Soc., 418, 2154
Fiorucci M., Tosti G. & Rizzi N., 1998, PASP 110, 105
Fomin, V. P., et al. 1994, Astropart. Phys., 2, 137
Ghisellini, G., Tavecchio, F. & Chiaberge M. 2005, A&A, 432, 401.
Ghisellini, G., Tavecchio, F., Foschini, L., et al. 2010, MNRAS, 402, 497
Georganopoulos, M., & Kazanas, D., 2003, ApJ, 594, L27
Giannios, D., Uzdensky, D. A. & Begelman, M.C. 2010, MNRAS, 402. 1649
Giommi, P., et al. 2012, A&A 541, 160
Goetting, N., et al. 2001, Proc. of 27th ICRC, Hamburg, 2669
Henri, G. & Saugé L. 2006 ApJ, 640, 185
Hillas, A. M. 1985, Proc. of 19th ICRC, La Jolla, 445
Kataoka, J., et al. 2010, ApJ, 715, 554
Krichbaum, T. P., et al. 1992, A&A, 260, 33
Lenain, J.-P., et al. 2008, A&A, 478, 111
Li, T.-P., & Ma, Y.-Q. 1983, ApJ, 272, 317
Lister, M. L., et al. 2009, The Astronomical Journal, 137, 3718
Lombardi, S., et al. 2011, Proc. of 32nd ICRC, Beijin, China, August 2011, arXiv:1109.6195
Lynds, R. 1970, ApJLetters, 159, L151
Maraschi, L., & Tavecchio, F. 2003, ApJ, 593, 667
Nagai, H., et al. 2010, Publ. Astron. Soc. Japan, 62, L11
Nagai, H., et al. 2012, Mon. Not. R. Astron. Soc. 423, L122
Nagai, H., et al. 2013, Publ. Astron. Soc. Japan, 65, 24
Nilsson, K., et al. 2007, A&A, 475, 199
Nolan, P. L., Abdo, A. A., Ackermann, M., et al. 2012, ApJS, 199, 31
Planck Collaboration; Ade, P. A. R. et al. 2011, A&A, 536, 7
Pedlar, A., et al. 1990, Mon. Not. R. astr. Soc. 246, 477
Perkins, J. S., et al. 2006, ApJ, 644, 148
Pinzke, A. & Pfrommer, C. 2010, MNRAS 409, 2, 449
Reimer, O., at al. 2003, ApJ, 588, 155
Rieger, F. M. & Mannheim, K. 2002, A&A, 396, 833
Rolke, W. A., López, A. M., & Conrad, J. 2005, Nucl. Instrum. Meth., A551, 493
Schlegel, D. J., Finkbeiner, D. P., & Davis, M. 1998, ApJ, 500, 525
Seyfert, C. K. 1943, ApJ, 97, 28.
Sironi, L., & Spitkovsky, A. 2011, ApJ, 726, 75
Strong A. W. & Bignami G. F. 1983 ApJ, 274, 549
Tavecchio, F., Maraschi, L., & Ghisellini, G. 1998, ApJ, 509, 608
Tavecchio, F., & Ghisellini, G. 2008, MNRAS, 385, L98
Tavecchio F., Ghisellini G., Ghirlanda G., Foschini L., Maraschi L., 2010, MNRAS, 401, 1570
Urry, C. M., & Padovani, P. 1995, PASP, 107, 803
Vermeulen, R. C., Readhead, A. C. S. & Backer, D. C. 1994, ApJ, 430, L41
Veron, P. 1978, Nature 272, 430
Walker, R. C., Romney, J. D. & Benson, J. M. 1994, ApJ, 430, L45

---

[1] IFAE, Edifici Cn., Campus UAB, E-08193 Bellaterra, Spain
[2] Università di Udine, and INFN Trieste, I-33100 Udine, Italy
[3] INAF National Institute for Astrophysics, I-00136 Rome, Italy
[4] Università di Siena, and INFN Pisa, I-53100 Siena, Italy
[5] Croatian MAGIC Consortium, Rudjer Boskovic Institute, University of Rijeka and University of Split, HR-10000 Zagreb, Croatia
[6] Max-Planck-Institut für Physik, D-80805 München, Germany
[7] Universidad Complutense, E-28040 Madrid, Spain
[8] Inst. de Astrofísica de Canarias, E-38200 La Laguna, Tenerife, Spain
[9] University of Lodz, PL-90236 Lodz, Poland
[10] Deutsches Elektronen-Synchrotron (DESY), D-15738 Zeuthen, Germany
[11] ETH Zurich, CH-8093 Zurich, Switzerland
[12] Universität Würzburg, D-97074 Würzburg, Germany
[13] Centro de Investigaciones Energéticas, Medioambientales y Tecnológicas, E-28040 Madrid, Spain
[14] Technische Universität Dortmund, D-44221 Dortmund, Germany
[15] Inst. de Astrofísica de Andalucía (CSIC), E-18080 Granada, Spain
[16] Università di Padova and INFN, I-35131 Padova, Italy
[17] Università dell'Insubria, Como, I-22100 Como, Italy
[18] Unitat de Física de les Radiacions, Departament de Física, and CERES-IEEC, Universitat Autònoma de Barcelona, E-08193 Bellaterra, Spain
[19] Institut de Ciències de l'Espai (IEEC-CSIC), E-08193 Bellaterra, Spain
[20] Finnish MAGIC Consortium, Tuorla Observatory, University of Turku and Department of Physics, University of Oulu, Finland
[21] Japanese MAGIC Consortium, Division of Physics and Astronomy, Kyoto University, Japan
[22] Inst. for Nucl. Research and Nucl. Energy, BG-1784 Sofia, Bulgaria
[23] Universitat de Barcelona (ICC/IEEC), E-08028 Barcelona, Spain
[24] Università di Pisa, and INFN Pisa, I-56126 Pisa, Italy
[25] now at Ecole polytechnique fédérale de Lausanne (EPFL), Lausanne, Switzerland
[26] now at Department of Physics & Astronomy, UC Riverside, CA 92521, USA
[27] now at Finnish Centre for Astronomy with ESO (FINCA), Turku, Finland
[28] also at Instituto de Fisica Teorica, UAM/CSIC, E-28049 Madrid, Spain
[29] Now at Stockholms universitet, Oskar Klein Centre for Cosmoparticle Physics
[30] now at GRAPPA Institute, University of Amsterdam, 1098XH Amsterdam, Netherlands
[31] INAF - Osservatorio Astrofisico di Torino, Strada Osservatorio 20, 10025 Pino Torinese, Italy
[32] Waseda University, Tokyo, Japan